Charge transfer of 0.5-, 1.5-, and 5-keV protons with atomic oxygen: Absolute differential and integral cross sections

B. G. Lindsay, D. R. Sieglaff, D. A. Schafer, C. L. Hakes, K. A. Smith, and R. F. Stebbings
Department of Physics, Department of Space Physics and Astronomy, and Rice Quantum Institute, Rice University, Post Office Box 1892, Houston, Texas 77251
(Received 10 July 1995)

We report measurements of the absolute differential cross sections for charge-transfer scattering of 0.5-, 1.5-, and 5-keV protons by atomic oxygen at scattering angles between 0.01° and 2.6° in the laboratory frame. Absolute integral cross sections are also reported and compared with previously published total cross sections. The measurements were made using a flowing gas target, which consisted of a mixture of atomic and molecular oxygen produced by passage of O_2 through a microwave discharge. The cross sections for atomic oxygen were obtained by appropriate subtraction of the signal due to molecular oxygen from that due to the mixture of O and O_2.

PACS number(s): 34.70.+e, 34.50.Lf

I. INTRODUCTION

Atomic and molecular collisions are of fundamental physical interest and play a central role in a wide range of environments. Laboratory measurements of collision cross sections can supply the information necessary for the accurate modeling of these environments. The data presented here are of particular relevance to proton auroras in which significant fluxes of keV protons precipitate into the earth's upper atmosphere. The basic collision cycle undergone by these protons is charge exchange followed by stripping, followed by charge exchange, etc.,

$$H^+ + M \rightarrow H + M^+, \tag{1}$$

$$H + M \rightarrow H^+ + M + e^-, \tag{2}$$

where $M = O, O_2, N_2$.

As a result of this neutralization-reionization cycle the initial proton flux becomes a mixture of protons and fast neutral atoms. While the protons are geomagnetically confined, the hydrogen atoms formed by charge transfer have no such restriction and in consequence the precipitating particles spread out over a large region of space [1]. The behavior of the auroral protons therefore depends critically on the magnitude of these cross sections. While laboratory data for both processes are available for N_2 and O_2 targets the only published studies involving atomic oxygen, the major atmospheric constituent between 200 and 600 km, are for process (1) and the most recently published data [2] disagree with the earlier work [3,4] by a factor of 2. A further quantity required to model this process accurately is the angular distribution of the scattered neutral charge-transfer products as this influences how far precipitating fluxes penetrate into the atmosphere [5]. Measurements of angular distributions for charge-exchange scattering of protons by N_2 and O_2 have been reported previously [6], and the current study extends those measurements to include the much more technically difficult case of atomic oxygen.

II. APPARATUS AND EXPERIMENTAL METHOD

A schematic of the scattering apparatus is shown in Fig. 1. Positive ions emerging from a low-pressure plasma-type ion source containing hydrogen are accelerated to the desired energy and focused by an electrostatic lens. The proton beam is then mass selected by a pair of 60° sector magnets and passes through a collimating aperture before traversing the target cell. A position-sensitive detector (PSD) on the beam axis 26 cm beyond the target cell is used to monitor both the primary ion beam and the fast neutral collision products. The pressure in the target cell is chosen to ensure that single-collision conditions obtain; when the target cell contains only a single species, the differential cross section for charge exchange is given by

$$\frac{d\sigma(\theta)}{d\Omega} = \frac{\Delta S(\theta)}{Snl\Delta\Omega}, \tag{3}$$

where S is the primary ion beam flux, $\Delta S(\theta)$ is the neutral flux scattered at angle θ into a solid angle $\Delta\Omega$, n is the target number density, and l is the target cell length. $\Delta S(\theta)$ is de-

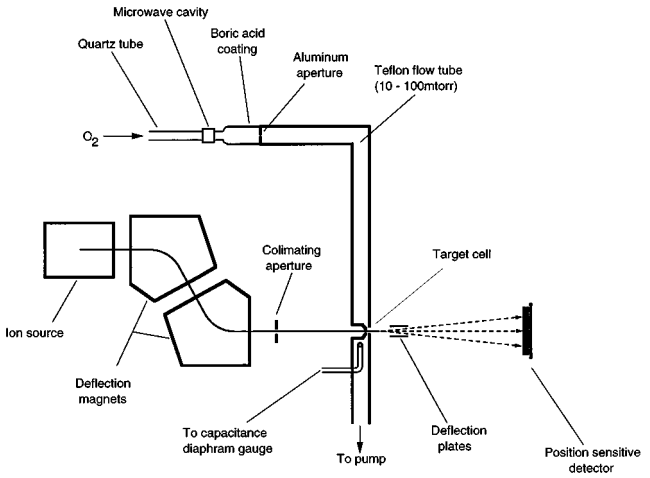

FIG. 1. Overview of the scattering apparatus.

termined by applying a transverse electric field to deflect the proton beam after it passes through the target cell, thereby allowing only the neutral collision products to impact the PSD. To measure the ion-beam flux (typically a few thousand particles per second) this field is momentarily removed. The resulting flux of ions and neutrals is equal to S, the flux of ions entering the target cell. The PSD output is therefore a measure of S because, as discussed below, the ions and neutral atoms are detected with the same efficiency. During this measurement, the ion beam is rastered over a 0.5 cm $\times$ 0.5 cm square on the detector to ensure that the detection efficiency is not impaired by saturation effects that occur when only a few microchannels are impacted by an intense highly-collimated ion beam [7]. As indicated in Eq. (3), cross-section determination involves measurement of the ratio of the fluxes of the primary ions and neutral products. Previous studies in this laboratory [8,9] have shown that the ion and neutral detection efficiencies are identical to within the experimental uncertainties at 5 keV, while at 1.5 keV and 0.5 keV they are the same to within 5% and 10%, respectively. In this work therefore we take $\Delta S/S$ as equal to the ratio of the neutral signal to the ion signal recorded by the PSD.

Detection of a particle causes the PSD electronics to generate a pair of digitized (eight-bit) coordinates for the particle impact position together with an indication that new, valid data are present. The laboratory computer, a Macintosh Quadra 800, then increments the element of a 256$\times$256 array whose coordinates correspond to the digitized PSD output. The array in the computer memory therefore is a histogram, the base of which represents the detector surface, and the height represents the number of particles striking each 110 μm $\times$ 110 μm pixel on the PSD surface. Since the target species are not oriented in any way, the product scattering pattern is symmetric about the beam axis. The origin of the coordinate system for analysis of the scattering is therefore identified with the center of mass of the histogram and the detector area is partitioned into a set of rings concentric with this origin. Most of the detector pixels lie entirely within a specific ring. However, whenever a pixel spans the border between two rings, the counts in that pixel are apportioned between the rings according to the fraction of the pixel area falling on each of the respective rings. The angular displacement of each ring and the solid angle it subtends at the target cell are established by the apparatus dimensions and the position calibration of the detector. Two files recording the primary beam flux, the target cell pressure, and the histogram of counts on the PSD surface are obtained: one with the target cell evacuated and one with target gas present. Effects due to scattering by residual gas and apertures are removed by appropriate subtraction of these two files.

The relatively short target cell length, approximately 1 mm, ensures that the scattering occurs within a very well defined location, thereby enabling accurate definition of the scattering angles of the neutral products. In order to obtain a satisfactory signal level while ensuring single-collision conditions, the target pressure was maintained at about 10 mTorr. The cell entrance and exit apertures are laser drilled in 25-μm-thick tantalum disks and are 20 and 300 μm in diameter, respectively. The separation between them is measured prior to assembly of the flow system by aligning a microscope so that its optical axis coincides with the beam axis in the cell and repetitively focusing the microscope on each aperture. The motion of the microscope's objective lens required to shift its focus from one aperture to the other is measured with a dial indicator. Despite the short cell length and the large diameter of the exit aperture it has been demonstrated by earlier studies in this laboratory [10] that the target thickness is accurately represented by the product of l, the physical length of the cell, and n, the number density of the target gas, which is obtained from a measurement of the target gas pressure using a capacitance diaphragm gauge.

III. CROSS-SECTION MEASUREMENTS FOR ATOMIC OXYGEN

A number of studies have been completed in this laboratory involving chemically stable target gases and cross sections obtained by use of Eq. (3) have been reported. In the present investigation this approach has necessarily been modified because a source of pure oxygen atoms of sufficient density is not currently achievable. In consequence, a microwave discharge source has been developed that provides a target comprising an admixture of oxygen atoms and molecules. It is no longer possible therefore to determine the number density of the target species using a capacitance diaphragm gauge; instead the composition of the target gas is obtained by mass spectrometric analysis of the gas emerging from the exit aperture of the target cell. In addition to the development of an O-atom source this experimental approach thus requires assessment of the target composition together with a method for explicit determination of the signal due to scattering of the protons by the atomic oxygen component of the target.

A. The target cell and flow system

As shown in Fig. 1, pure O_2 emerging from a metering valve enters a 10-mm-diam quartz tube that traverses a microwave cavity driven by a 300-W source at 2.45 GHz. The microwave field sustains a discharge in which the O_2 is partially dissociated. The resulting mixture of gases passes through a 10 cm length of 23-mm-diam boric-acid-coated quartz tubing and a 1.27-mm-diam oxidized aluminum aperture into a 2.5-cm-diam, 40-cm-long Teflon tube that leads to the target cell. These materials are utilized because recombination of atomic oxygen is observed to be relatively slow on both boric-acid-coated quartz and Teflon surfaces. The pressure inside the quartz tube is maintained at about 0.2 Torr, which both ensures a stable discharge and permits cooling of the gas mixture via multiple gas phase and wall collisions in the tubulation downstream of the cavity. The pressure decreases considerably as the gas passes through the aluminum aperture and continues to fall along the length of the flow tube, reaching a value of typically 10 mTorr at the target cell. The mean time required for a particle to travel from the discharge region to the target cell is approximately 0.3 sec, as determined by measurement of the flow system throughput and pressure. During this time collisional and radiative effects lead to a significant reduction in the excited-state contamination of the target. Cooling of the gas also reduces the rate of chemical reaction between the flowing gas and the Teflon tube; in the absence of the high-pressure buffer zone, provided by the boric-acid-coated quartz tube, significant

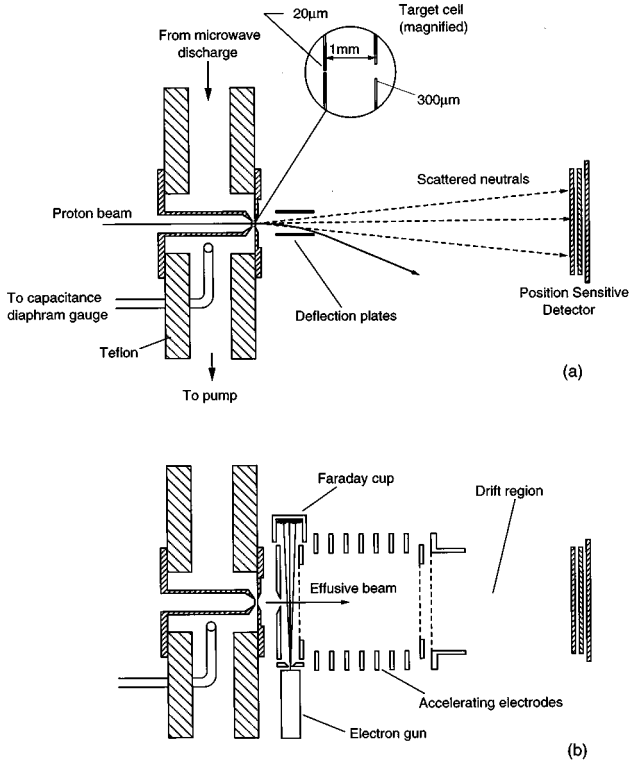

FIG. 2. Apparatus schematic: (a) scattering mode and (b) mass spectrometer mode.

concentrations of CO and CO_2 products from reaction of the flow gas with the Teflon tubulation were observed. After passing through the target cell, the gas is carried to a Welch 1397 two-stage mechanical pump (500-l/min free air displacement).

B. The mass spectrometer

When the target comprises a single species, as is the case when the discharge is off, it is only necessary to ensure that the gas being admitted to the cell is uncontaminated and to measure its pressure. The O_2 used in this experiment was obtained from Matheson Gas Products and has a minimum specified purity of 99.98%. The target number density is obtained from the target pressure, as measured by an MKS Baratron capacitance diaphragm gauge connected to the target cell by 60 cm of 4-mm-diam tubing. A correction of approximately 2% is necessary to account for thermal transpiration [11].

When the discharge is ignited, resulting in a multicomponent target, the number density of each species is determined using a time-of-flight mass spectrometer. This spectrometer, which comprises a pulsed electron gun, accelerating, and field-free drift regions, is moved into the location shown in Fig. 2(b) for this purpose, thus displacing the deflection plates used in the scattering mode. The electron-beam current is monitored by a Faraday cup, biased to suppress secondary-electron emission, and a picoammeter whose output is read by an analog to digital converter interfaced to the laboratory computer. Some of the gas effusing from the target cell exit aperture enters the mass spectrometer, where it is ionized by a 1-μS-wide electron beam pulse and the resulting ions extracted by a pulsed electric field, which is applied across the ionization region 2 μS after the electron beam pulse. After passing through acceleration and drift regions, which are biased to time focus the ions [12], they impact the PSD. At 20-sec intervals the effusive beam entering the ionization region from the target cell is blocked by a beryllium-copper shutter (not shown) and the ion signal then results entirely from the background gas. Subtraction of the ''shutter open'' time-of-flight spectrum from the ''shutter closed'' spectrum yields the time-of-flight spectrum due only to ionization of the gas emerging from the target cell as shown in Fig. 3. The mass analyzed parent ion signal S_p for a given species is then related to N_p, the number density of the neutral parent in the gas cell, by

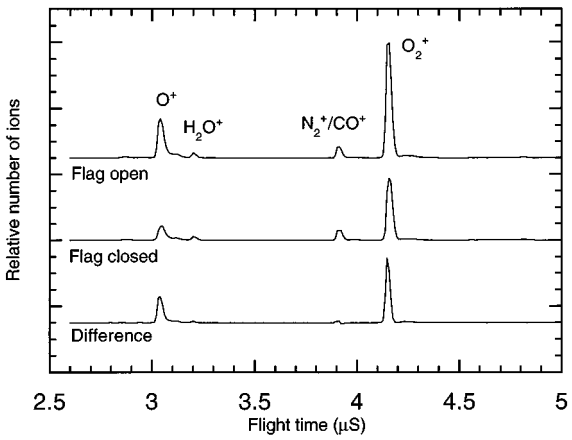

FIG. 3. Representative time-of-flight spectra.

$$\frac{S_p}{I_e} = kN_p\sigma, \tag{4}$$

where I_e is the electron current, σ is the electron-impact ionization cross section, and k is an instrumental constant. For specific settings of the mass spectrometer k should clearly be independent of the target species and indeed measurements carried out in this laboratory with several of the rare gases served to demonstrate this independence. These considerations do not apply to fragment ions such as O^+ from O_2 since they may be formed with appreciable kinetic energy and will be collected with a lower efficiency. In the present investigation k is determined from Eq. (4) by passing pure O_2 through the target cell while measuring the number density of O_2 in the cell with a baratron capacitance manometer.

When the microwave discharge is ignited the $O_2{}^+$ signal obtained with the mass spectrometer yields the, now reduced, number density of O_2 through

$$N_{O_2} = \frac{S_{O_2{}^+}}{k\sigma_{O_2} I_e}. \tag{5}$$

The situation is more complicated for atomic oxygen because O^+ ions formed by dissociative ionization of O_2 contribute to the observed O^+ signal. This contribution is readily determinable from the measurements with pure O_2 and after

TABLE I. Absolute cross-section values used in the evaluation of the H^+-O cross sections, where E is the projectile energy. The charge transfer data are integral cross sections over the angular range 0°–2.6°.

Process	Cross section (Å^2) $E=200$ eV	$E=500$ eV	$E=1.5$ keV	$E=5$ keV	Reference
$e+O_2\rightarrow O_2^+ +2e$	1.45				[27]
$e+O\rightarrow O^+ +2e$	1.24				[13]
$e+H_2O\rightarrow H_2O^+ +2e$	1.21				present work
$H^+ +O_2\rightarrow H+O_2^+$		13.7	10.3	9.0	present work
$H^+ +H_2O\rightarrow H+H_2O^+$		19.8	16.5	12.4	present work

its subtraction the residual O^+ signal then gives the O-atom number density in the target through

$$N_O=\frac{S_{O^+}}{k\sigma_O I_e}. \quad (6)$$

Implicit in this analysis is the requirement that all ion species are detected by the PSD with the same absolute efficiency. Earlier studies demonstrated [7] that, at the 3-keV impact energy used here, ions of mass up to that of atomic oxygen have a detection efficiency that is numerically equal to the ratio of the open area of the detector's channels to the total detector area. In other words, every ion that enters a microchannel is detected. As part of the present investigation these detection efficiency measurements were extended and it was determined that at this 3-keV impact energy O_2^+ ions are also detected with the same efficiency as the lighter ions. Use of a position-sensitive detector permitted verification that all the ions of interest were being collected.

Two tests were conducted to confirm that the Faraday cup used to collect the electron beam was operating correctly. One of these involved varying the cup suppression voltage and the other consisted of sweeping the 200-eV electron beam across the cup to confirm that the entire beam was entering the cup aperture. In order to measure absolute target densities with the mass spectrometer, it is necessary to know the relevant electron-impact ionization cross sections. Because of perceived deficiencies in the previously published values, a remeasurement of the cross sections for O_2 and H_2O was carried out in this laboratory (see Table I). The electron-impact ionization cross section for atomic oxygen used in this study was that measured by Harrison and coworkers [13].

IV. COMPOSITION OF THE MIXED TARGET

The gas target typically comprised approximately 74% molecular oxygen, 24% atomic oxygen, 1.5% water vapor, and 0.5% molecular nitrogen and carbon monoxide. The water vapor originates from the boric acid coating in the discharge tube, while the carbon monoxide component is due to reaction of the atomic oxygen with the Teflon flow tube. It is possible to reduce the percentage of water vapor, but at the cost of a considerable reduction in the atomic oxygen density. In consequence, the approach adopted here was to work with some water vapor contamination and to make allowance for its effect on the scattering measurement.

In addition to the production of ground-state $O(^3P)$ atoms, excited oxygen atoms and molecules are formed in the microwave discharge. The collisional quenching rate for $O(^1D)$ in O_2 has been measured by Germany, Salmo, and Anderson [14] and that for $O(^1S)$ by Atkinson and Welge [15]. Quenching rates for $O(^1S)$ in O and $O_2(a\,^1\Delta_g)$ are also known [16,17]. That for $O_2(b\,^1\Sigma_g^+)$ has been measured by Arnold and Ogryzlo [18] for wall collisions and by Slanger and Black [17] for gas phase collisions. The rates are such that all of these metastable species have a sufficiently short lifetime in the flow system that they do not reach the target cell. Molecules in the $O_2(a\,^1\Delta_g)$ metastable state may, however, survive the journey from the discharge and be present in the target cell and clearly the success of this experiment hinges in part on our ability to correctly assess their possible influence. To this end a series of tests was carried out at sufficiently high pressures that the O-atom population was largely depleted by recombination. The collisional quenching rates for $O_2(a\,^1\Delta_g)$ are sufficiently small [19,20] that this species is not significantly quenched in these circumstances. Thus, with the discharge off, the flow was pure ground state O_2, while with the discharge on, the flow comprised ground-state O_2 plus some admixture of $O_2(a\,^1\Delta_g)$. The charge-transfer cross section for protons with the oxygen molecules was determined both with the discharge off and on. The measured cross sections were found to agree to within better than 1%, indicating that either no significant population of $O_2(a\,^1\Delta_g)$ was in fact present or that its charge-transfer cross section is the same as that for the ground state. Similar checks with the mass spectrometer, performed at 10 and 20 times the normal operating pressure, demonstrated no measurable effects due to excited molecules. Finally, the observed invariance of the charge-transfer cross sections measured under various discharge conditions further indicated that excited species have negligible influence on the present results.

V. DERIVATION OF THE H^+-O CROSS SECTIONS

To determine the cross section for charge exchange between H^+ and O it is necessary to measure the H^+ scattering from the O, O_2, and H_2O gas mixture. The number densities of O, O_2, and H_2O in the cell are determined with the mass spectrometer by use of Eq. (4) with the aid of the electron-impact ionization cross sections listed in Table I. The contributions to the charge-transfer scattering from the O_2 and H_2O in the mixture are then subtracted from the total signal using their known charge-transfer cross sections. The remaining signal is then due to charge exchange between H^+ and O and the differential charge-transfer cross section may be evaluated by Eq. (3).

For a single-component target, where the target pressure

TABLE II. Laboratory-frame differential charge-transfer cross sections for H^+-O collisions, where E is the projectile energy and the numbers in square brackets represent powers of 10.

Laboratory angle θ (deg)	$\frac{d\sigma(\theta)}{d\Omega}$ (Å^2 sr^{-1}) $E=500$ eV	$E=1.5$ keV	$E=5$ keV
0.012	2.61[5]	8.37[5]	1.86[6]
0.036	2.89[5]	7.57[5]	1.25[6]
0.059	2.56[5]	5.36[5]	6.64[5]
0.083	1.96[5]	2.88[5]	2.49[5]
0.107	1.29[5]	1.35[5]	1.04[5]
0.130	8.04[4]	8.97[4]	5.65[4]
0.154	4.56[4]	7.38[4]	3.45[4]
0.178	3.62[4]	5.46[4]	1.66[4]
0.202	3.31[4]	3.35[4]	7.69[3]
0.225	3.93[4]	2.03[4]	5.89[3]
0.249	3.53[4]	1.34[4]	4.62[3]
0.273	2.63[4]	1.14[4]	4.06[3]
0.297	1.77[4]	1.14[4]	2.34[3]
0.320	1.13[4]	8.19[3]	1.57[3]
0.344	9.40[3]	6.16[3]	1.49[3]
0.368	9.22[3]	4.42[3]	1.24[3]
0.415	1.00[4]	3.49[3]	9.26[2]
0.486	6.19[3]	2.49[3]	5.84[2]
0.557	3.01[3]	1.73[3]	3.82[2]
0.629	2.53[3]	1.04[3]	2.82[2]
0.700	1.67[3]	8.04[2]	2.60[2]
0.771	1.47[3]	5.50[2]	2.04[2]
0.842	8.29[2]	4.34[2]	2.00[2]
0.913	7.41[2]	3.23[2]	2.07[2]
0.984	5.81[2]	2.08[2]	1.18[2]
1.056	6.11[2]	1.53[2]	7.64[1]
1.127	4.08[2]	1.16[2]	1.30[2]
1.198	2.81[2]	1.12[2]	1.27[2]
1.269	1.26[2]	9.06[1]	9.62[1]
1.340	2.03[2]	5.16[1]	6.35[1]
1.411	1.41[2]	6.74[1]	7.65[1]
1.506	1.42[2]	5.50[1]	7.79[1]
1.625	1.00[2]	4.01[1]	5.97[1]
1.744	9.48[1]	4.96[1]	4.06[1]
1.862	4.52[1]	3.68[1]	6.55[1]
1.981	7.93[1]	2.67[1]	4.72[1]
2.099	6.06[1]	1.96[1]	3.20[1]
2.218	3.63[1]	1.86[1]	3.59[1]
2.337	3.05[1]	1.67[1]	3.04[1]
2.455	3.81[1]	1.05[1]	2.04[1]
2.574	3.16[1]	1.99[1]	2.53[1]

can be measured directly, the uncertainties in the absolute integral cross sections are approximately 6% at 5 and 1.5 keV and 11% at 500 eV. These errors, which are considered in more detail in a previous publication [21], are in large part due to the uncertainty in the ratio of ion to neutral detection efficiencies mentioned earlier. In the present case, because of the inherent difficulties associated with the target number density determination, the absolute uncertainty is significantly greater. The absolute accuracy of the present data is 20% at 5 and 1.5 keV and 22% at 0.5 keV.

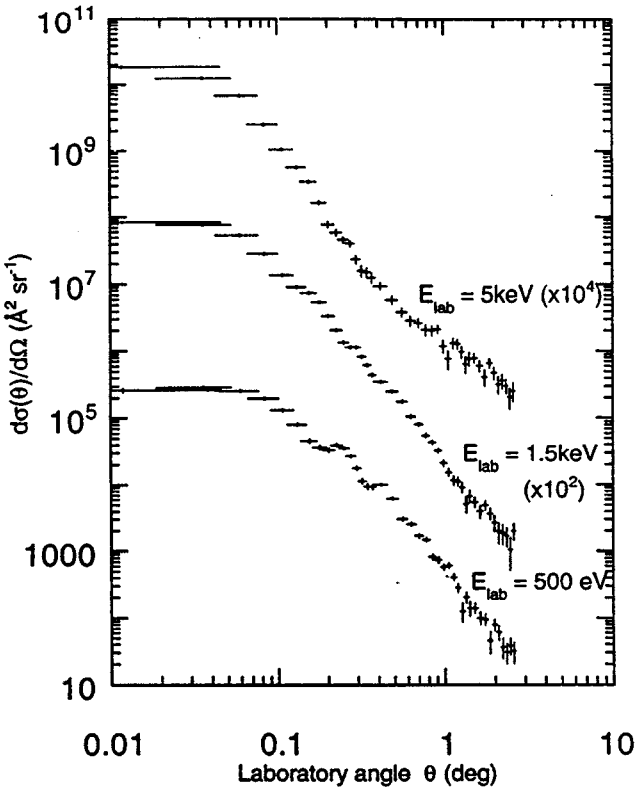

FIG. 4. Differential cross sections for charge-transfer scattering of H^+-O at projectile energies of 0.5, 1.5, and 5 keV. Note that, for clarity, the 1.5- and 5-keV data are shown on different scales.

VI. RESULTS AND DISCUSSION

The differential H^+-O charge-transfer cross sections for 0.5, 1.5, and 5 keV are shown in Fig. 4 and tabulated in Table II. The vertical error bars in the figure represent the statistical error. The horizontal error bars arise from the finite primary beam size and the ''ring'' width used for analysis and are thus primarily an indication of the angular resolution of the measurement. As has been observed for other near resonant processes, the differential cross sections are strongly peaked in the forward direction. As the impact energy is increased the cross section becomes slightly more forward peaked, as would be expected from simple momentum transfer considerations. The presence of the large-angle scattering component, observed in the highest-energy differential cross section, may be due to the opening of more nonresonant channels. The structure at 0.25°, which can only be clearly seen in the 0.5-keV cross section, is probably due to a combination of classical trajectory effects and quantum interference. Similar but more pronounced undulations have been observed previously in proton–rare-gas differential cross sections [8]. No other experimental or theoretical data exist with which to compare these differential cross sections. Several previous studies of total cross sections have been reported, however, and all the available experimental data are shown in Fig. 5. The experiments fall into two broad

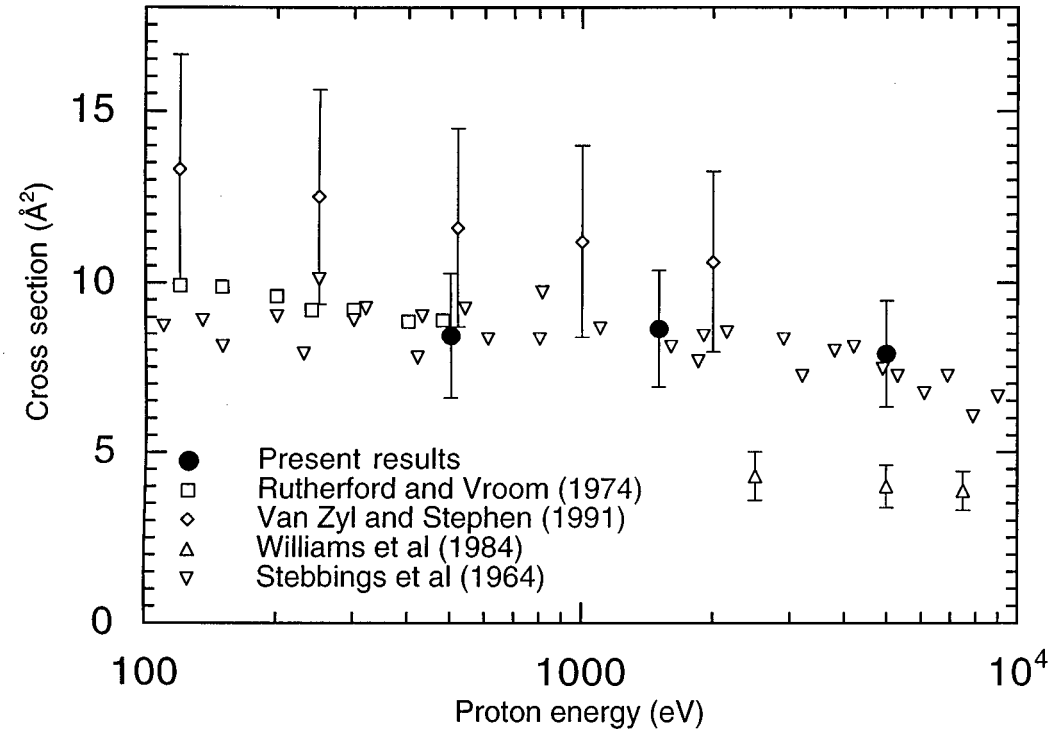

FIG. 5. Absolute H^+-O integral charge-transfer cross sections.

classes: those in which the cross section is determined from measurements of the slow product ions and those in which the fast neutral products are detected. In principle, those two approaches lead to the same result. However, whereas it is relatively straightforward to collect all the slow ions, measurements of the fast neutral products typically fail to detect particles that are scattered outside an apparatus-dependent angle. In the present experiment that angle is about 2.6°, while in the experiments of Williams, Geddes, and Gilbody [2] and Van Zyl and Stephen [22] it is 4°. Inspection of the differential cross sections shown in Fig. 4 demonstrates, however, that the fraction of the total cross section that is missed in these measurements is small and it is appropriate therefore to directly compare the results of the two classes of measurement.

A major difficulty in all these experiments is the production and analysis of the atomic oxygen target and it is here that discrepancies between different investigations are most likely to arise. In the original investigation of Stebbings, Smith, and Ehrhardt [3] molecular oxygen was partially dissociated in a rf discharge. A beam comprising oxygen atoms and molecules effused from a narrow slit in the wall of the discharge-containing glass vessel and the degree of dissociation was determined by observation of the reduction of the molecular oxygen content of the beam when the rf was applied. Constant mass flow in the beam was assumed, permitting determination of the atomic oxygen content. It was recognized that long-lived excited atoms and molecules would be present in the beam and various procedures were adopted to minimize their possible influence. The authors nonetheless noted that their results may have been influenced by the presence of metastable species in the neutral beam.

In the three remaining studies [2,4,22], the oxygen atoms were obtained by thermal dissociation of molecular oxygen in an iridium furnace, which largely eliminates the possibility of excited states of O and O_2 in the beam. Different furnace designs were utilized in these studies, but all were constructed of iridium and were heated to approximately 2100 K. Rutherford and Vroom and Williams, Geddes, and Gilbody [2] again inferred the dissociation fractions of the beams emerging from their furnaces by measurement of the reduction in the molecular oxygen content, assuming constant mass flow. This is probably a safe assumption, but not entirely without risk since oxidation reactions could conceivably deplete the gas flow. This notwithstanding, the measurements of Rutherford and Vroom are in excellent accord with those presented here and with those of Stebbings, Smith, and Ehrhardt while the results of Van Zyl and Stephen, who made a more direct determination of the dissociation fraction [23], also agree to within the combined uncertainties.[1] Thus there would appear to be no problems inherently associated with the choice either of a thermal or of a discharge source for the O atoms.

The results of Williams, Geddes, and Gilbody, however, fall substantially below all the remaining data. They apparently were unaware of the work of Rutherford and Vroom and suggested that their disagreement with the results of Stebbings, Smith, and Ehrhardt was attributable to excited-state effects experienced by the latter. This explanation was,

[1]The agreement is in fact better than the figure suggests because Van Zyl and Stephen actually measured the ratios of the cross sections for H^+ impact on O and O_2 and subsequently normalized their relative data to the H^+-O_2 cross section. Their H^+-O data in Fig. 5 lie above ours, in part, because they normalized their O-atom data to the H^+-O_2 cross sections of Koopman [24], which are significantly larger than our own measurements (Table I).

and remains, plausible and could be invoked also to account for the discrepancy between the present results and those of Williams, Geddes, and Gilbody. It cannot, however, explain the discrepancy between the results of Williams, Geddes, and Gilbody and those of Rutherford and Vroom and of Van Zyl and Stephen.[2] Finally, it should be noted that the thermal energy measurement of Fehsenfeld and Ferguson [26] is also consistent with an, admittedly long, extrapolation to lower energies of the higher cross-section values.

[2]Recent measurements [25] reported by Thompson, Shah, and Gilbody after the submission of this paper have resulted in a revision of the 1984 data of Williams, Geddes, and Gilbody upward by about a factor of 2 and the recent results are in very good agreement with those reported here.

VII. SUMMARY

Differential cross sections for charge exchange between protons and oxygen atoms are reported. The results are of fundamental interest and are intended for inclusion in atmospheric models. Integral cross sections obtained from these data are in good agreement with three of the four previous measurements of the total cross section.

ACKNOWLEDGMENTS

This work was supported by the Robert A. Welch Foundation and the National Science Foundation, Atmospheric Sciences Section. We would like to acknowledge useful discussions with R. S. Gao, H. C. Straub, B. Van Zyl, and R. E. Johnson.

[1] G. T. Davidson, J. Geophys. Res. **70**, 1061 (1965).
[2] I. D. Williams, J. Geddes, and H. B. Gilbody, J. Phys. B **17**, 1547 (1984).
[3] R. F. Stebbings, A. C. H. Smith, and H. Ehrhardt, J. Geophys. Res. **69**, 2349 (1964).
[4] J. A. Rutherford and D. A. Vroom, J. Chem. Phys. **61**, 2514 (1974).
[5] M. Ishimoto, M. R. Torr, P. G. Richards, and D. G. Torr, J. Geophys. Res. **91**, 5793 (1986).
[6] R. S. Gao, L. K. Johnson, C. L. Hakes, K. A. Smith, and R. F. Stebbings, Phys. Rev. A **41**, 5929 (1990).
[7] R. S. Gao, P. S. Gibner, J. H. Newman, K. A. Smith, and R. F. Stebbings, Rev. Sci. Instrum. **55**, 1756 (1984).
[8] L. K. Johnson, R. S. Gao, C. L. Hakes, K. A. Smith, and R. F. Stebbings, Phys. Rev. A **40**, 4920 (1989).
[9] R. S. Gao, L. K. Johnson, D. A. Schafer, J. H. Newman, K. A. Smith, and R. F. Stebbings, Phys. Rev. A **38**, 2789 (1988).
[10] J. H. Newman, K. A. Smith, and R. F. Stebbings, J. Geophys. Res. **90**, 11 045 (1985).
[11] K. F. Poulter, M. J. Rodgers, P. J. Nash, T. J. Thompson, and M. P. Perkin, Vacuum **33**, 311 (1983).
[12] W. C. Wiley and I. H. McLaren, Rev. Sci. Instrum. **26**, 1150 (1955).
[13] E. Brooke, M. F. A. Harrison, and A. C. H. Smith, J. Phys. B **11**, 3115 (1978); R. G. Montague, M. F. A. Harrison, and A. C. H. Smith, *ibid*. **17**, 3295 (1984).
[14] A. Germany, G. J. Salmo, and R. J. Anderson, J. Appl. Phys. **54**, 4573 (1983).
[15] R. Atkinson and K. H. Welge, J. Chem. Phys. **57**, 3689 (1972).
[16] W. Felder and R. A. Young, J. Chem. Phys. **56**, 6028 (1972).
[17] T. G. Slanger and G. Black, Geophys. Res. Lett. **8**, 535 (1981).
[18] S. J. Arnold and E. A. Ogryzlo, Can. J. Phys. **45**, 2053 (1967).
[19] *Reaction Rate and Photochemical Data for Atmospheric Chemistry—1977*, edited by Robert F. Hampson, Jr. and David Garvin, NBS Special Publ. No. 513 (U.S. GPO, Washington, DC, 1978).
[20] I. D. Clark and R. P. Wayne, Chem. Phys. Lett. **3**, 405 (1969)
[21] G. J. Smith, L. K. Johnson, R. S. Gao, K. A. Smith, and R. F. Stebbings, Phys. Rev. A **44**, 5647 (1991).
[22] B. Van Zyl and T. M. Stephen, in *Abstracts of Contributed Papers of the Seventeenth International Conference on the Physics of Electronic and Atomic Collisions, Brisbane, 1991*, edited by I. E. McCarthy, W. R. MacGillivray, and M. C. Standage (Hilger, Bristol, 1992).
[23] B. Van Zyl (private communication).
[24] D. W. Koopman, Phys. Rev. **166**, 57 (1968).
[25] W. R. Thompson, M. B. Shah, and H. B. Gilbody (unpublished).
[26] F. C. Fehsenfeld and E. E. Ferguson, J. Chem. Phys. **56**, 3066 (1972).
[27] H. C. Straub, P. Renault, B. G. Lindsay, K. A. Smith, and R. F. Stebbings (unpublished).